Int. J. Heat Mass Transfer. Vol. 32, No. 5, pp. 895–911, 1989
Printed in Great Britain

0017–9310/89 $3.00+0.00

A study of traveling wave instabilities in a horizontal channel flow with applications to chemical vapor deposition

GREG EVANS
Computational Mechanics Division, Sandia National Laboratories, Livermore, CA 94550, U.S.A.

and

RALPH GREIF
Mechanical Engineering Department, University of California, Berkeley, CA 94720, U.S.A.

(*Received* 2 *May* 1988 *and in final form* 3 *October* 1988)

Abstract—The flow and heat transfer of helium in a horizontal channel of height H and length L with a heated bottom surface and a cooled top surface are studied. Numerical solutions of the transient, two-dimensional Navier–Stokes and energy equations reveal that for conditions of interest in chemical vapor deposition (CVD), a thermal instability in the fluid (the Rayleigh–Benard instability), produced by the temperature difference between the horizontal surfaces of the channel, can result in traveling, transverse waves. The results show the effects of these waves on the flow and the heat transfer over a range of Reynolds numbers, $Re = \bar{u}H/\nu_0$ ($10^{-1} < Re < 10^2$), Grashof numbers, $Gr = g\varepsilon H^3/\nu_0^2$ ($2.5 \times 10^3 < Gr < 6.0 \times 10^5$), aspect ratios, L/H ($4 < L/H < 50$), for two temperature ratios, $\varepsilon = (T_s - T_0)/T_0$, 0.0333 and 2.333, corresponding to constant and variable property flow, respectively. The existence of transverse, traveling waves is shown to enhance the heat transfer from 50 to more than 300% over the condition without traveling waves. The important effect of the aspect ratio on the results is also emphasized.

INTRODUCTION

CHEMICAL vapor deposition (CVD) is an important process for fabricating micro-electronic components. Although widely used, the CVD process is not very well understood and, as a result, reactor design is often based on empirical methods. In the CVD process, a mixture of reacting and inert gases, e.g. silane and helium, flows over a heated substrate. As the heat is transferred from the substrate by convection and by diffusion, the active gas pyrolyzes to form species that are reactive on the substrate. Reactant gases are transported to the heated substrate where surface reactions produce a solid deposit (e.g. silicon). A volatile product is released into the flowing gas and carried out of the reaction chamber. Many reactor geometries are used in CVD, and a horizontal channel flow CVD reactor is shown in Fig. 1.

Some of the important quantities of interest in the fabrication of semiconductors with CVD are the rate of the deposition, the uniformity of the deposition, and the sharpness of the interfaces between adjacent layers. Several of the parameters which can be controlled are the reactor geometry, the flow rates of the gases through the reactor, the flow rate distributions at the inlet of the reactor, the thermal boundary conditions on the surfaces of the reactor, the temperature of the substrate, and the composition of the reactant gas mixture.

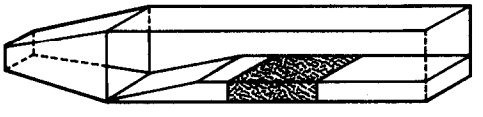

FIG. 1. Example of a horizontal channel CVD reactor.

Fluid flow and convective heat transfer play important roles in the CVD process as noted by Jensen [1], Giling [2], Coltrin *et al.* [3] and Ostrach [4]. The transport processes give rise to boundary layers that often lead to non-uniform deposition on the heated substrate and, depending upon the orientation and temperature of the reactor surfaces, buoyancy effects can be significant. As a result, thin, highly uniform deposits which also have sharp interfaces can be difficult to obtain.

In general, the prediction of deposition rates and distributions in a CVD reactor requires the solution of the three-dimensional, time-dependent equations for the conservation of mass, momentum, and energy in the reactor geometry of interest. Furthermore, a chemical reaction mechanism is required to describe both the gas phase and the surface chemistry. Boundary conditions as well as constitutive relationships for shear stress, heat flux and mass diffusion flux are also required. The complete solution of CVD problems is not feasible at present due to limitations of computer hardware and software. However, for some condi-

NOMENCLATURE

c_p	specific heat
D	substantial derivative
Gr	Grashof number, $g\varepsilon H^3/\nu_o^2$
g	acceleration of gravity
H	channel height
k	thermal conductivity
L	channel length
$Nu_{b,t}$	local Nusselt numbers on bottom and top surfaces, $q^*_{b,t}H/(k_o(T_s-T_o)) = -k(\partial\Theta/\partial y)\|_{y=0,1}$
$\overline{Nu}_{b,t}$	average Nusselt numbers on bottom and top surfaces, $\overline{q^*_{b,t}}H/(k_o(T_s-T_o)) = H/L\Sigma_{b,t}Nu_{b,t}$
n_i	unit gravitational vector
Pr	Prandtl number, $\nu_o/\alpha_o = 2/3$ for helium
p	pressure
$\hat{p}$	pressure due to motion in momentum equations
$Q^*_{b,t}$	total dimensional heat flow rate from bottom and top surfaces, $\Sigma_{b,t}q^*_{b,t}\Delta x$
$q^*_{b,t}$	dimensional local heat flux at bottom and top surfaces, $-k^*(\partial T/\partial y^*)\|_{y^*=0,1}$
$\overline{q^*_{b,t}}$	dimensional average heat flux at bottom and top surfaces, $Q^*_{b,t}/L$
Ra	Rayleigh number, $g\varepsilon H^3/(\nu_o\alpha_o) = Gr\,Pr$
Re	Reynolds number, $\bar{u}H/\nu_o$
T	temperature
t	time
u	horizontal velocity
$\bar{u}$	average dimensional horizontal velocity at inlet of channel
u_{tw}	dimensional speed of thermal waves, $\bar{u}(\sqrt{(Gr)}/Re)(\lambda/\tau)$
v	vertical velocity
W	channel width
x	horizontal coordinate
Δx	grid spacing in x-direction
y	vertical coordinate.

Greek symbols

α	thermal diffusivity
β	dimensional coefficient of thermal expansion, $1/T_o$
δ_{ij}	Kronecker delta
ε	temperature ratio, $(T_s-T_o)/T_o$
Θ	dimensionless temperature, $(T-T_o)/(T_s-T_o)$
λ	wavelength of transverse traveling waves
μ	dynamic viscosity
ν	kinematic viscosity
ρ	density
τ	period of transverse traveling waves.

Subscripts and superscripts

o	dimensional quantities evaluated at temperature T_o and to conditions at cold surface of channel ($y = 1$)
s	conditions at hot surface of channel ($y = 0$)
*	dimensional quantity.

tions and reactor geometries, CVD problems can be simplified to one-dimensional or partial two-dimensional (boundary layer approximation) problems, and several investigations of this type have been made [3, 5, 6].

For completeness it is pointed out that some three-dimensional aspects of CVD have recently been studied [7]. Moffat and Jensen [8, 9] solved the steady-state, parabolized heat, momentum and mass-transfer equations for variable property, mixed convection in a horizontal channel. They included finite rate chemistry in the dilute reactant formulation which is discussed below.

In many CVD problems the fluid mechanics and heat transfer can be separated from the chemistry and species transport. The reactants often appear as trace species in an inert carrier gas; consequently predictions of the flow field and the heat transfer can be made by solving multidimensional conservation equations for a single species. Furthermore, the deposition is often limited by convection and diffusion processes in the gas phase [10, 11], and for those situations in which the analogy between heat and mass transfer is valid, the uniformity and magnitude of the deposit can be obtained directly from the solution of the energy equation for the carrier gas. If the analogy cannot be made, e.g. due to different boundary conditions for species and temperature, thermal diffusion effects, etc., then the species equations must be solved to obtain the deposition rates.

The gas flow in CVD reactors is characterized by small Mach and Reynolds numbers. The density and other properties undergo significant changes due to the large temperature differences and the Boussinesq approximation (density constant everywhere except in the body force term) is not valid. Although the gas flow in many CVD reactors is often assumed to be steady, transient instabilities may be induced by thermal or by other effects.

THE HORIZONTAL CHANNEL FLOW REACTOR

An idealized horizontal channel flow reactor is shown in Fig. 2. The channel height, H, is usually a few

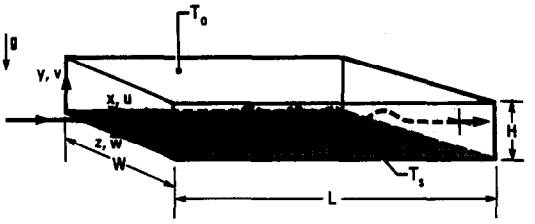

FIG. 2. Horizontal channel geometry and coordinate system. The analysis is for the two-dimensional geometry.

centimeters, the channel length, L, is approximately 1 m, and the width, W, is approximately 10 cm. Although not shown in Fig. 2, an unheated entrance length may be present to allow for hydrodynamic development of the flow. A heated substrate, $T_s \approx$ 1000–1300 K, which is several centimeters to several tens of centimeters in length, forms the lower surface of the channel. The carrier gas is usually hydrogen or an inert gas such as helium, argon, or nitrogen. At the channel inlet, the average flow velocity, $\bar{u}$, is typically a few centimeters per second.

The Reynolds number of these flows, based on the height of the channel and the average velocity, $Re = \bar{u}H/\nu_0$, varies from 1 to 1600 (typically around 20). The Grashof number, based on the channel height and the temperature difference between the lower and upper surfaces of the channel, $Gr = g\varepsilon H^3/\nu_0^2$, with the properties evaluated at the reference temperature, T_0, varies from 50 to 1.0×10^7 with a typical value being 10^5. Research in convective heat transfer (referred to in the next section) has shown that the flow in a horizontal channel can have a varied structure depending primarily on the relative effects of inertia and buoyancy which appear in the ratio: Re^2/Gr. For values of Re^2/Gr that are typical in CVD (10^{-3}–10^{-1}), buoyancy effects on the flow field and on the convective heat transfer are expected to be very important. Secondary flow instabilities can occur ranging from transverse, traveling waves that are oriented at right angles to the main flow to steady, longitudinal rolls that are aligned with the main flow. In both cases the heat transfer rate from the substrate to the gas is increased significantly (when the instability is present), and hence the deposition rate would also be increased. However, in the former case the instability sweeps through the channel at a rate that is related to the value of Re^2/Gr whereas in the latter the instability remains stationary. Thus, these instabilities would be expected to produce dramatically different effects on the uniformity and thickness of the deposited material. Although transient instabilities have been mentioned in several studies on CVD [12, 13] the most recent models of the flow in a horizontal channel typical of CVD conditions [8, 9, 14], have been restricted to steady flow and have resulted in steady, longitudinal rolls.

Summary of related research

Laminar flows in horizontal channels that are heated from below have been studied both experimentally and analytically with most of the emphasis being placed on the condition where the buoyant forces are small compared to the inertial forces (large values of Re^2/Gr), e.g. Mori and Uchida [15], Akiyama *et al.* [16], Kamotani and Ostrach [17], Incropera and Schutt [18]; however, a few studies have considered $Re^2/Gr < 0.1$ [19, 20]. To date, most of the experimental results are for small temperature differences only and almost all of the analytical and numerical studies have used the Boussinesq approximation. An exception to this is the numerical study of Moffat and Jensen [8] in which the steady, parabolized Navier–Stokes equations for variable properties were solved for mixed convection in a horizontal channel.

For $Re^2/Gr = 0$, there is no imposed flow through the channel and provided the Rayleigh number is greater than the critical value, convection rolls will occur. For a rectangular box with no imposed flow, Davis [21] in a theoretical study and Stork and Müller [22] in an experimental study showed that the thermal instability associated with heating on the lower surface is manifested in the form of rolls with axes aligned parallel with the short dimension of the box. In typical CVD channel geometries (cf. Fig. 1), the short side of the channel is perpendicular to the direction of the flow.

The studies concerned with small Re^2/Gr (<0.1) can be divided into two groups: Couette flow and Poiseuille flow in horizontal channels heated from below. Chandra [23] carried out a Couette flow experiment in a duct where the upper cooled plate was moved relative to the lower stationary heated plate. He found that transverse waves appeared for small shear rates. For larger shear rates, these transverse waves were replaced by longitudinal rolls. Similar findings in Couette flow were later observed by Brunt [24], who observed that as the shear rate was reduced (as Re^2/Gr was decreased from 0.66 to 0.35) the flow pattern switched from longitudinal rolls to transverse waves.

In an analysis of the linearized equations, Gage and Reid [25] examined the three-dimensional stability of a thermally stratified plane Poiseuille flow of infinite horizontal extent. They found that for Rayleigh numbers greater than the critical value of 1708 the flow was unstable ($Ra = g\varepsilon H^3/(\nu_0\alpha_0) = Gr\,Pr$, where Pr is the Prandtl number; Gage and Reid considered only the $Pr = 1$ case). Depending on the values of Re and Ra, the flow was unstable to disturbances varying from transverse waves, the axes of which were perpendicular to the main flow direction, to longitudinal rolls that were aligned with the main flow. Platten and Legros [26] investigated analytically buoyant convection in horizontal channel flows of finite lateral extent. They determined the Ra–Re region in which the flow field consists of traveling, transverse waves. In an experimental study, Luijkx *et al.* [27]

demonstrated the existence of traveling, transverse waves in a channel with $W/H = 5$, that was heated from below and cooled from above with a fully developed Poiseuille velocity profile for the initial condition. As the Reynolds number was increased, these transverse waves eventually were replaced by longitudinal rolls.

Recently, Chiu and Rosenberger [12] determined experimentally the thermal entry lengths for the onset of instability and the development of the flow of nitrogen in a horizontal channel with an inlet parabolic flow profile for $1368 < Ra < 8300$, $15 < Re < 170$, and $W/H = 10$. They observed steady longitudinal rolls for $Re^2/Gr = 0.3$; however, for combinations of large Ra and small Re ($Re^2/Gr \approx 0.03$), they noted that the longitudinal rolls were unsteady and indicated that the effect was due to a combination of transverse, traveling waves and longitudinal rolls.

The previous studies have shown that, provided Ra is above a critical value and Re is sufficiently small, transverse traveling waves occur in a channel flow that is heated from below. As Re^2/Gr is increased much greater than 0.1 (for $Pr \approx 1$), the transverse, traveling waves are replaced by longitudinal rolls, as noted above by Chandra [23] and Brunt [24] for Couette flow and Luijkx *et al.* [27] for Poiseuille flow, although in Luijkx *et al.* [27] the transition occurs at much smaller values of Re^2/Gr due to the effects of the large Prandtl number (450) used in their study. For very large values of Re^2/Gr, the flow is dominated by forced convection. It is emphasized that the values of Re^2/Gr that are typical for CVD are within the regime of transverse traveling waves.

We have developed and applied a model using the two-dimensional transient Navier–Stokes equations to examine thermal instabilities in CVD reactors. We have determined that transverse, traveling wave instabilities can sweep periodically through a horizontal channel reactor from inlet to outlet. These results are new and, as noted above, may be very important for the operation of CVD reactors.

GOVERNING EQUATIONS

The conservation equations for mass, momentum and energy are the basic equations governing the behavior of a fluid continuum. We assume that the pressure in the system is large enough for the continuum equations to be valid. This is true for most applications of CVD. However, at pressures of only a few Torr, although the continuum assumption is valid, the assumption that the fluid flow and the heat transfer in the carrier gas are separable from the reacting species is no longer valid since the reacting species now form a large fraction of the gas in the system. Thus, the applicability of our present results to CVD is limited to those situations in which the carrier gas is the dominant species.

The geometry under consideration is shown in Fig. 2. The equations are made dimensionless with the following scales: channel height H, characteristic velocity $\sqrt{(g\beta(T_s - T_o)H)}$, time $\sqrt{(H/(g\beta(T_s - T_o)))}$, pressure $\rho_o g\beta(T_s - T_o)H$, and temperature difference $T_s - T_o$ with $\Theta = (T - T_o)/(T_s - T_o)$, where T_s and T_o are the temperatures of the bottom and top surfaces of the channel, respectively. The fluid properties are made dimensionless with the values evaluated at the temperature T_o, designated by the subscript 'o'. We again emphasize that the Boussinesq approximation is not made.

The dimensionless equations for an ideal gas are

$$\frac{\partial \rho}{\partial t} + \frac{\partial(\rho u_j)}{\partial x_j} = 0 \tag{1}$$

$$\frac{\partial(\rho u_i)}{\partial t} + \frac{\partial}{\partial x_j}(\rho u_j u_i) = -\frac{\partial \hat{p}}{\partial x_i} + \frac{(\rho - 1)}{\varepsilon} n_i + Gr^{-1/2}\frac{\partial \tau_{ij}}{\partial x_j} \tag{2}$$

$$\frac{\partial(\rho\Theta)}{\partial t} + \frac{\partial}{\partial x_j}(\rho u_j \Theta) = Gr^{-1/2} Pr^{-1}\left[\frac{\partial}{\partial x_j}\left(\frac{k}{c_p}\frac{\partial \Theta}{\partial x_j}\right) + \frac{k}{c_p^2}\frac{\partial \Theta}{\partial x_j}\frac{\partial c_p}{\partial x_j}\right] \tag{3}$$

$$\rho = \frac{\rho_s}{\rho_s(1 - \Theta) + \Theta} \tag{4}$$

where

$$x_i = (x, y, z);$$

$$\tau_{ij} = \mu\left(\frac{\partial u_i}{\partial x_j} + \frac{\partial u_j}{\partial x_i}\right) - \frac{2}{3}\delta_{ij}\mu\frac{\partial u_k}{\partial x_k};$$

$$\varepsilon = (T_s - T_o)/T_o.$$

In equations (2) and (4) we have utilized the results of a small Mach number expansion of the pressure [28]. The leading order term in this expansion is only a function of time which we have taken to be constant for the open channel flow considered. The first term on the right-hand side of equation (2) contains $\hat{p}$ which is the next higher order term of the Mach number expansion and is the dimensionless pressure due to motion. The hydrostatic component of the pressure and the body force are included in the second term on the right-hand side of equation (2) where n_i is the unit gravitational vector. In energy equation (3), viscous dissipation and compressibility effects associated with Dp/Dt are ignored and the Prandtl number Pr is defined as ν_o/α_o. In equation (4) ρ_s is the dimensionless gas density, evaluated at the temperature of the heated lower surface.

We restrict the analysis to the following conditions: (1) the flow is two-dimensional, i.e. $W \to \infty$, and (2) the axial velocity, u, is assumed to have a fully developed parabolic profile initially and at the channel entrance, $x = 0$. For small temperature differences ($\varepsilon = 0.0333$) a temperature profile that varies linearly from the bottom to the top of the channel is applied at the channel entrance whereas for large tempera-

ture differences ($\varepsilon = 2.333$) an adiabatic condition is applied at $x = 0$ since a linear temperature profile is not strictly valid in this case due to the effects of variable properties. However, it is pointed out that the results prove to be only slightly affected by the choice of the thermal boundary condition at $x = 0$. The initial temperature profile is assumed to vary linearly from the bottom to the top throughout the channel.

Specifically, the initial and boundary conditions are:

at $t = 0$

$$u = 6(Re/Gr^{1/2})(y-y^2), \quad v = 0, \quad \Theta = 1-y, \quad \text{for } 0 \leqslant x \leqslant L/H, 0 \leqslant y \leqslant 1; \quad (5)$$

for $t > 0$

$$u = 6(Re/Gr^{1/2})(y-y^2), \quad v = 0,$$

$$\Theta = 1-y \quad \text{or} \quad \frac{\partial \Theta}{\partial x} = 0, \quad \text{for } x = 0, \quad 0 \leqslant y \leqslant 1$$

$$\frac{\partial u}{\partial x} = \frac{\partial v}{\partial x} = \frac{\partial \Theta}{\partial x} = 0, \quad \text{for } x = L/H, \quad 0 \leqslant y \leqslant 1$$

$$u = v = 0, \quad \Theta = 1, \quad \text{for } 0 \leqslant x \leqslant L/H, \quad y = 0$$

$$u = v = \Theta = 0, \quad \text{for } 0 \leqslant x \leqslant L/H, \quad y = 1. \quad (6)$$

Note that the velocity scaling has been chosen to analyze flows with small values of Re^2/Gr. The five parameters in the above equations and boundary conditions are: Re, Gr, Pr, ε, and L/H.

NUMERICAL SOLUTIONS

Solution method and determination of accuracy

Equations (1)–(4) with initial conditions (5) and boundary conditions (6) are integrated over control volumes and finite differences are used to discretize the derivatives. A central difference formulation is used for all spatial derivatives and a backward Euler method is applied to the time derivatives. The solution method is semi-implicit and is based on the TEACH code [29]. The method is semi-implicit because the solution algorithm consists of a sequential line relaxation procedure, which is repeated until convergence criteria are satisfied. The momentum and energy equations are solved implicitly along lines that are normal to the channel surfaces and the equation for pressure is solved implicitly along lines both normal and parallel to the channel surfaces in an alternating fashion. The SIMPLER method described by Patankar [30] is used to determine the pressure field. Under-relaxation factors of 0.9 and 0.8 are used in the solution of the momentum and energy equations, respectively. There is no under-relaxation of the pressure equation. At each time step, in order to obtain an accurate transient solution, the equations are iterated until the following convergence criteria are achieved: at each grid point and for each dependent variable, the relative change from one iteration to the next must be less than 1 part in 10^5 and the absolute change must be less that 1 part in 10^6. Once these iteration criteria have been achieved for all of the dependent variables, a check is then made of the relative and absolute changes of all of the dependent variables at all of the grid points from the preceding time to the current time. If any variable at any grid point changes by more than 10% between time steps, the result is rejected, the current value of the time step is halved and the computation is repeated for the new current time. The residuals of the equations (absolute values summed over the grid and normalized by the number of control volumes) are also checked and typical values at convergence are between 10^{-4} and 10^{-5}. Global energy and momentum balances are maintained to better than 1% at each time step.

The sufficiency of these criteria has been checked. As an example, for a case of $Re = 30$, $Gr = 1.85 \times 10^5$, $L/H = 8$, $\varepsilon = 2.333$, helium ($Pr = 2/3$), negligible changes in the local heat flux at the surfaces of the channel occurred when the relative and the absolute error tolerances were changed from 10^{-5} and 10^{-6} to 10^{-6} and 10^{-7}, respectively. It has also been demonstrated that the results are essentially independent of the time step criterion.

The sensitivity of the results to the grid size and the time step have also been obtained. As an example, for the parameters described in the preceding paragraph, an (x, y) grid of (81, 21) points with an initial time step of 0.2, which was subsequently reduced to 0.1, was used. The change in the local surface heat flux when the number of y grid points was doubled to 41 was between 2 and 3%. A similar change occurred when the number of x grid points was increased from 81 to 121. No discernible differences in the local heat flux occurred when the time step was decreased from 0.1 to 0.05.

Results for small temperature differences

In the limit of $L/H \to \infty$, with constant properties and a temperature profile that varies linearly at $x = 0$ from the lower hot surface to the upper cold surface, the present formulation reduces to the problem studied by Gage and Reid [25]. Their stability diagram is reproduced in Fig. 3 and is for $Pr = 1$. Curves of neutral stability for wave or roll instabilities with axes aligned at the designated angle to the z-axis (0.0° corresponds to traveling, transverse waves, 90.0° corresponds to stationary, longitudinal rolls) are shown. Note that the region above a given curve corresponds to an unstable flow. The flow is unstable to longitudinal roll instabilities provided that $Ra > 1708$, independent of Re. However, in respect to traveling, transverse waves (the axes of which are in the z-direction) the stability of the flow depends on both Ra and Re, approaching $Ra = 1708$ for small values of Re. According to Fig. 3, the flow is least stable to longitudinal rolls (90°) for all values of Re. However, Platten and Legros [26] and Luijkx *et al.* [27] have

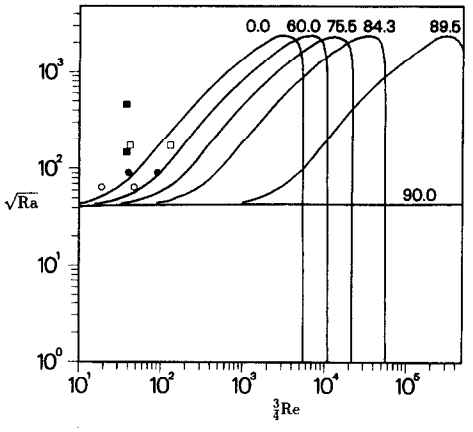

FIG. 3. Three-dimensional stability curve from Gage and Reid [25]. Curve labels correspond to orientation of instability: 0.0° for transverse waves, 90.0° for longitudinal rolls. Experimental data: ●, Chiu and Rosenberger [12]; ○, Akiyama *et al.* [16]; □, Kamotani and Ostrach [17]; ■, Kamotani *et al.* [19].

shown that for a channel with side walls, there is a critical value of Re below which the flow is least stable to traveling, transverse waves. Experimental data for convection in horizontal channels at small to moderate values of Re^2/Gr are also shown in Fig. 3. These data are within the Boussinesq limit. It is noted that Chiu and Rosenberger [12] obtained indirect evidence of traveling, transverse waves and Kamotani *et al.* [19] observed flow patterns that penetrated upstream.

We have solved the transient two-dimensional equations for flow in a horizontal channel with $L/H = 20$ in the Boussinesq limit ($\varepsilon = 0.0333$) for $Re = 0.1$ and $Pr = 2/3$, starting with an unstable case ($Ra = 6666$), and proceeding to smaller and smaller values of Ra until there is no longer an instability. For this small value of Re, which is actually off the left edge of Fig. 3, the flow should be unstable to transverse disturbances for all values of Ra that are slightly larger than 1708 (the critical value of Ra in the absence of a mean flow). Figure 4 shows the results for the local surface Nusselt numbers and the temperature field for several Ra. We note that the local Nusselt numbers are shown over the total channel, $L/H = 20$, whereas for clarity, the temperature field is only shown over the upstream half of the channel, $x \leqslant 10$. The local Nusselt numbers at the bottom and top surfaces of the channel are defined as

$$Nu_{b,t} \equiv \frac{q^*_{b,t} H}{k_o (T_s - T_o)} = -k \left.\frac{\partial \Theta}{\partial y}\right|_{y=0,1}. \tag{7}$$

The results were obtained in a sequence of calculations, starting with initial conditions (5) and $Ra = 6666$, and integrating equations (1)–(4) until the time average of the spatially averaged Nusselt numbers (defined below) on the lower and upper surfaces of the channel changed by less than 2%. We define stationarity to be the condition when the spatially

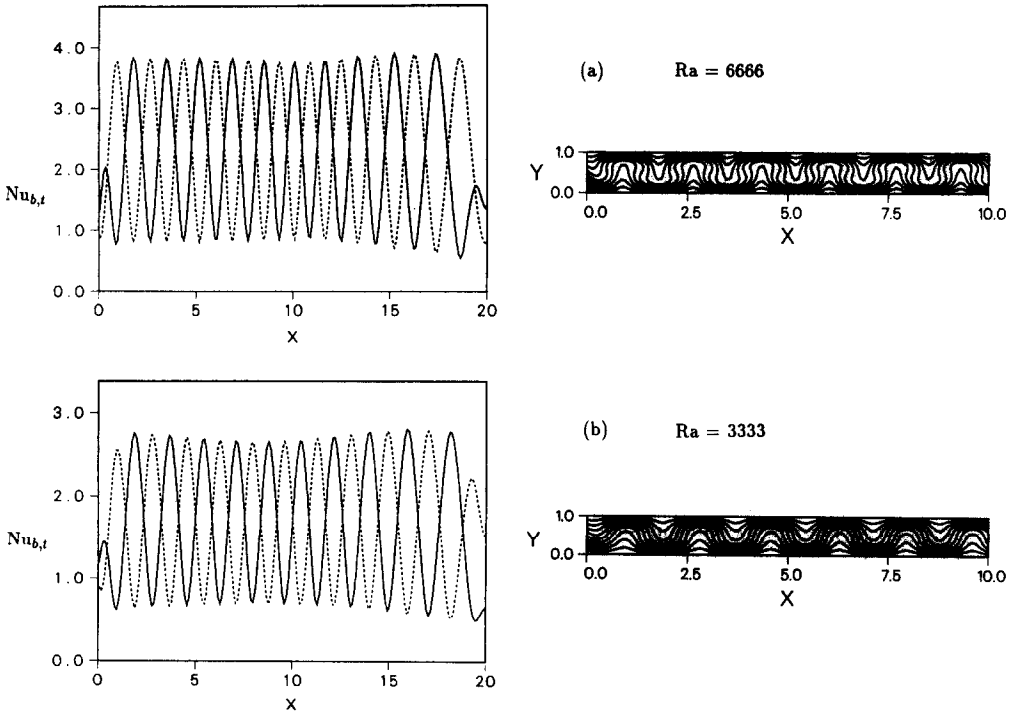

FIGS. 4(a) and (b). Heat fluxes from lower hot surface (——) and upper cold surface (– – –) of the channel and temperature fields in the upstream half of the channel for $Re = 0.1$, $L/H = 20$, $\varepsilon = 0.0333$: (a) $Ra = 6666$; (b) $Ra = 3333$.

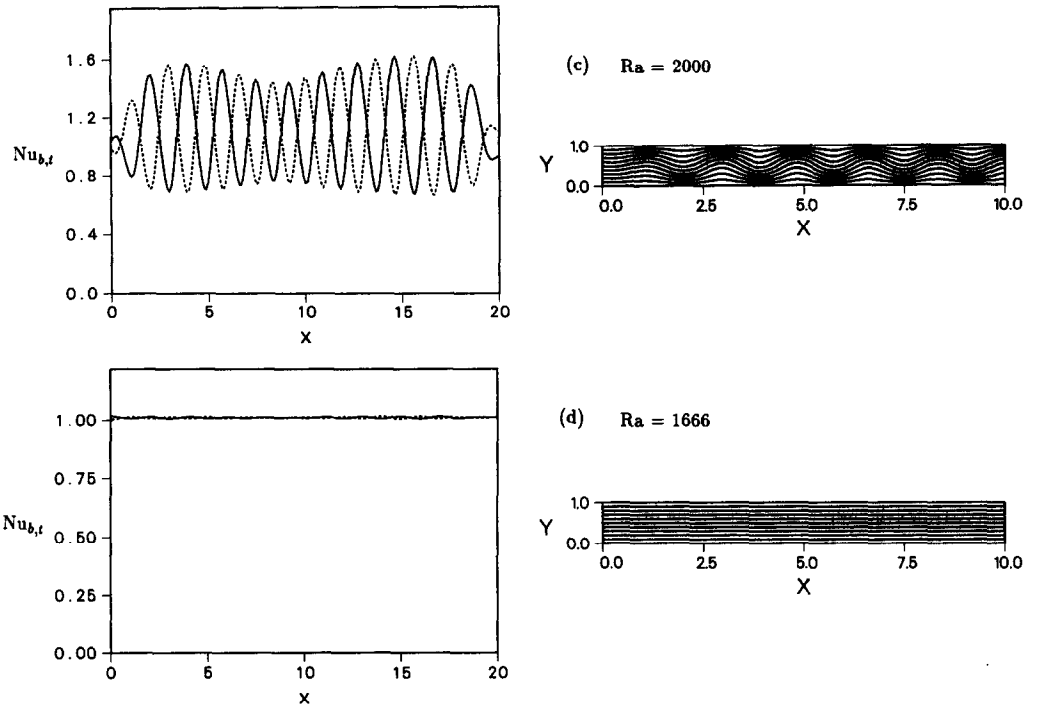

FIGS. 4(c) and (d). Heat fluxes from lower hot surface (——) and upper cold surface (– – –) of the channel and temperature fields in the upstream half of the channel for $Re = 0.1$, $L/H = 20$, $\varepsilon = 0.0333$: (c) $Ra = 2000$; (d) $Ra = 1666$.

averaged Nusselt numbers at the surfaces of the channel change by less than 2% over a time interval that is large compared to the characteristic time of the system. Because the transit time of the fluid through the channel is extremely long for the conditions of Fig. 4 ($Re = 0.1$), it is not possible to determine conclusively that the flow is stationary. However, we note that the wave pattern shown in Fig. 4(a) is much different from the initial conditions and is established rapidly, and further integration in time does not result in any noticeable changes. Once a result for a particular value of Ra was obtained, a new calculation was begun by lowering Ra, and the results at the previously higher value of Ra were used as the initial conditions.

In Fig. 4(a) the channel is filled with transverse waves with a dimensionless wavelength λ (defined to be the x-distance from peak to peak of the traveling waves) of slightly less than 2. In Fig. 4(b), $Ra = 3333$ and the heat flux is smaller; however, λ remains slightly less than 2. In Fig. 4(c), $Ra = 2000$ and the heat flux is again smaller; furthermore, the heat flux is reduced significantly in the center of the channel relative to the values both upstream and downstream. Finally, in Fig. 4(d), $Ra = 1666$ and the waves have disappeared. Note that the local Nusselt numbers are defined in equation (7) to yield a value of unity when a linear temperature gradient corresponding to heat conduction in a fluid with constant thermal conductivity exists between the horizontal surfaces. The results shown in Figs. 4(c) and (d) serve to bracket the onset of instability between the values of $Ra = 1666$ and 2000. This is in agreement with the value of Gage and Reid [25] which would be slightly larger than 1708 for the present case of $Re = 0.1$.

Zero gradient boundary conditions (6) are used often in the numerical computation of elliptic flows with open flow boundaries; however, they are only approximate conditions. As can be seen in Fig. 4, there is a clear effect of these boundary conditions within one wavelength of the exit of the channel. We have examined the effects of these conditions on the flow in the interior of the channel by comparing the variations of the local Nusselt number for several aspect ratios. The effects of the boundary conditions at $x = L$ on the flow in the interior should diminish as the aspect ratio is increased. Calculations were carried out for values of L/H varying from 10 to 30 for the parameters of Fig. 4(b) ($Ra = 3333$, $Re = 0.1$, $\varepsilon = 0.0333$). Over this range of aspect ratios, the amplitude and the wavelength of the local Nusselt number oscillations did not change within the uncertainty in the determination of these quantities which was about 10–15%. These quantities were determined by a simple measurement from Fig. 4(b) for $L/H = 20$ and from the corresponding figures (not shown) for the other L/H values. We emphasize that the accuracy of the calculations is much better than this uncertainty; specifically, as noted previously, the accuracy is between 2 and 3%.

We also examined the instability at $Re = 40$ by first calculating an unstable case ($Ra = 10^4$) and then pro-

ceeding to smaller Ra. According to Gage and Reid the flow should be unstable to transverse traveling waves for $Ra > 4900$. For $Ra = 10^4$ we obtained transverse, traveling waves which occurred in the downstream 60% of the channel for $L/H = 40$. This is shown in Fig. 5. Figure 5(a) shows the average Nusselt numbers for the hot and cold surfaces of the channel. The average Nusselt numbers are defined by

$$\overline{Nu}_{b,t} \equiv \frac{\overline{q^*_{b,t}} H}{k_o(T_s - T_o)} = H/L \sum_{b,t} Nu_{b,t}. \qquad (8)$$

Figure 5(b) shows the local Nusselt numbers on the two channel surfaces at $t = 200$. The instability consisting of transverse, traveling waves does not appear until $x > 10$. Note that the peak local heat flux in the region $x > 10$ (which can be seen in Fig. 5(b)) is more than three times larger than the value in the stable region $x < 10$, where the heat transfer is by conduction alone. Thus, for heat transfer enhancement, a tremendous advantage can be gained with a longer channel.

A separate simulation for $Ra = 10^4$ with $L/H = 15$ (not shown) showed signs of instability which disappeared at later time. Apparently, the aspect ratio was not large enough for the instability to remain. This might have been anticipated from Fig. 5(b) which shows that waves do not exist for $x/H < 10$.

Starting from the unstable case of Fig. 5, Ra was decreased to 6666 and the results for the average and the local Nusselt numbers are shown in Figs. 6(a) and (b). The instability is now confined to only the downstream half of the channel. A further decrease in Ra from 6666 to 5333 with $L/H = 40$ showed no signs of instability. The results for $Re = 40$ emphasize the effect of aspect ratio. As Ra is reduced for fixed Re the instability moves downstream. This phenomenon has been observed experimentally by Luijkx *et al.* [27]. As the critical value of Ra for transverse, traveling waves is approached starting from values of Ra that are above the critical value, the aspect ratio must become very large for the instability to be present. It appears that this occurs because the flow is sweeping the instability through the channel and a development length is required for the waves to be established. Thus, for small values of L/H the flow may not be unstable even though it would be for $L/H \to \infty$ (the case studied by Gage and Reid).

The ratio of the thermal wave speed to the average flow velocity in the channel, given by

$$u_{tw}/\bar{u} = \frac{\sqrt{(Gr)}}{Re} \frac{\lambda}{\tau} \qquad (9)$$

where λ and τ are the dimensionless wavelength and period of the thermal wave, respectively, has been

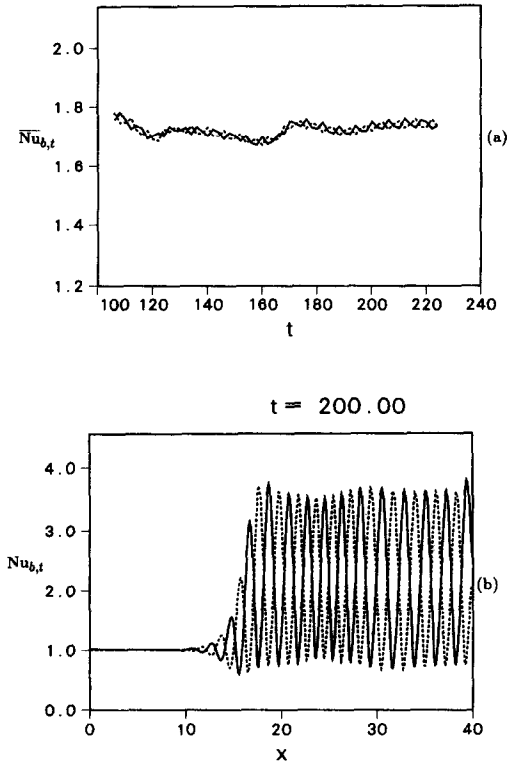

FIG. 5. Nusselt numbers from lower hot surface (——) and upper cold surface (– – –) of the channel for $Ra = 10^4$, $Re = 40$, $L/H = 40$, $\varepsilon = 0.0333$: (a) average Nusselt numbers; (b) local Nusselt numbers.

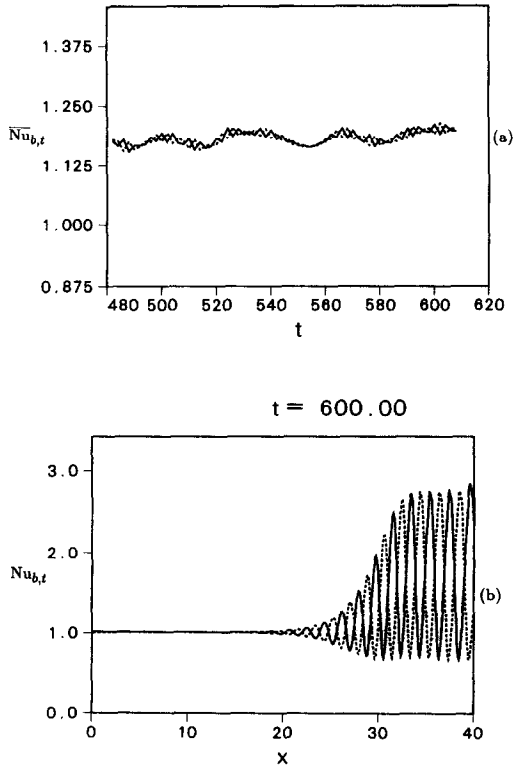

FIG. 6. Nusselt numbers from lower hot surface (——) and upper cold surface (– – –) of the channel for $Ra = 6666$, $Re = 40$, $L/H = 40$, $\varepsilon = 0.0333$: (a) average Nusselt numbers; (b) local Nusselt numbers.

determined. For the conditions of Fig. 5 ($Re = 40$, $Gr = 15000$), $u_{tw}/\bar{u} \approx 1.1$. Luijkx *et al.* [27] also determined that the transverse waves traveled faster than the average fluid velocity where $u_{tw}/\bar{u} = 1.38$ for the conditions of their experiment. For the results shown in Figs. 5 and 6, the time averages of the spatially averaged Nusselt numbers are constant to within 2%, and because Re is much larger than in Fig. 4, the time averages now correspond to one or more transits of the fluid through the unstable part of the channel. Thus, the results shown in Figs. 5 and 6 correspond to a stationary flow condition as defined earlier.

Results for large temperature differences

We now present results for variable property flow and heat transfer for helium in a horizontal channel for operating conditions that are typical of CVD processes. These results are similar to those discussed for constant properties in the preceding section. However, the thermal boundary condition at $x = 0$ is now $\partial\Theta/\partial x = 0$. Results for the temperature and velocity fields, the average Nusselt numbers on the hot and cold surfaces of the channel as a function of time, and the local Nusselt numbers on these surfaces at selected times are presented. All results are for a hot surface temperature of 1000 K and a cold surface temperature of 300 K, resulting in a value of $\varepsilon = 2.333$. The relations for the temperature dependence of the viscosity and thermal conductivity of helium are from kinetic theory expressions and are given in ref. [31]. The specific heat of helium at constant pressure is constant. We show how the results are affected by changes in Re, Gr, and L/H. Results are also presented for the temporal variation of the temperature at a selected location in the channel.

Nominal case. Figure 7 shows the results of the temperature and velocity fields in a horizontal channel after a steady, periodic flow has evolved with $Re = 30$, $Gr = 1.85 \times 10^5$, $Pr = 2/3$, $L/H = 8$, and $\varepsilon = 2.333$. Transverse waves traveling from left to right fill the entire channel. Frames from a computer generated movie are shown in Fig. 8. The temperature field is represented by color shading and the velocity field is represented by particle tracks. The movement of the thermal wave from left to right is shown in Figs. 8(a)–(d) at $t = 340$, 343, 346, and 349, respectively. Red, green, and blue correspond to high, intermediate, and low temperature regions of the flow, respectively. Figures 8(e)–(h) focus on the time interval between Figs. 8(a) and (b) and show the movement of the gas as represented by particle tracking at $t = 340$, 341, 342, and 343.

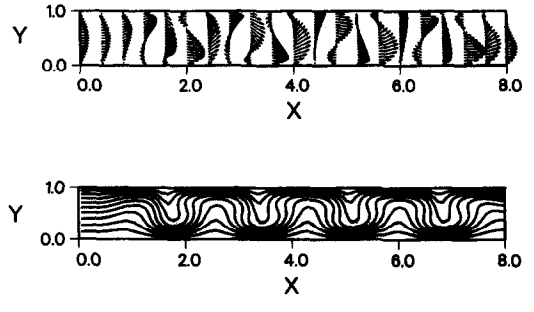

FIG. 7. Velocity and temperature fields in horizontal channel showing transverse waves traveling from left to right. $Gr = 1.85 \times 10^5$, $Re = 30$, $L/H = 8$, and $\varepsilon = 2.333$; waves are periodic.

Each string of 10 marker particles represents 10 successive positions of a single fluid particle as it traverses through the channel. The direction of motion of the fluid can be determined from the shade of the particle which fades from the black color representing the current fluid particle's position to the background color which represents the position of the same fluid particle at an earlier time. This technique allows visualization of the path of a fluid particle as well as yielding a direct measurement of the speed of the fluid since the distance between adjacent positions of the particle which represents the fluid particle's position at equal increments of time is directly proportional to the fluid speed. The particles are introduced into the channel at $x = 0$ at six equally spaced y positions with a frequency that allows for adequate flow visualization and replacement of the particles which exit the channel at $x = L$. In Figs. 8(e)–(h), the gas is seen to rise rapidly on the crest and the upstream side of the thermal wave and as the flow nears the top of the channel some of the gas turns downstream and then accelerates toward the bottom of the channel on the leeward side of the thermal wave while another portion of the gas turns and flows upstream before turning again and flowing toward the exit of the channel. There is significant recirculation of the gas within the channel; however these recirculation regions are correlated with the thermal waves and move with them from left to right in the channel. A more complete description of this flow field has been documented as a movie on videotape. A copy of the tape can be borrowed by contacting the first author.

A power spectral analysis of the temperature at a point in the middle of the channel has been performed and the frequency of these waves has been found to be ≈ 0.045. It is noted that the frequency associated with the vertical motion of the fluid as it traverses the sinusoidal path of dimensionless length 2.8 from the hot bottom surface of the channel to the cold top surface and back to the hot bottom surface is estimated to be: $v/2.8 \approx 0.047$, where $v = 0.13$ is a typical vertical speed in the channel. The temperature–time history at a point in the middle of the channel after a steady, periodic traveling wave condition has been established is shown in Fig. 9. The single frequency of the traveling waves is evident. The solution was obtained by using an (x, y) grid of (81, 21) points.

The average Nusselt numbers over the bottom and top surfaces of the channel are shown in Fig. 10 and appear to be periodic. The periodic variations in the average Nusselt numbers are a function of the aspect

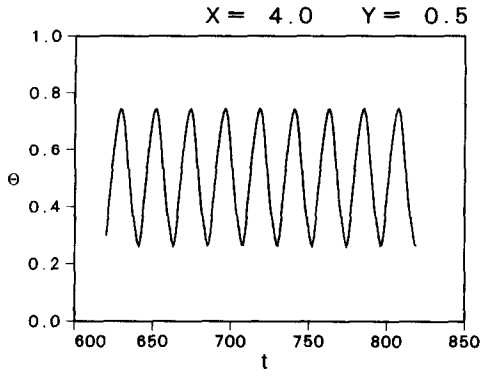

FIG. 9. Temperature–time history in the middle of the channel ($x = 4.0, y = 0.5$), once the steady, periodic traveling waves have occurred. $Gr = 1.85 \times 10^5$, $Re = 30$, $L/H = 8$, and $\varepsilon = 2.333$.

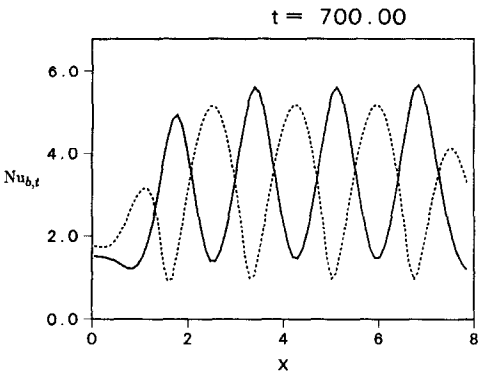

FIG. 11. Local Nusselt numbers along the lower hot surface (——) and the upper cold surface (– – –) of the channel for $t = 700$. The traveling waves are periodic and regular at this time (see Fig. 10). $Gr = 1.85 \times 10^5$, $Re = 30$, $L/H = 8$, and $\varepsilon = 2.333$.

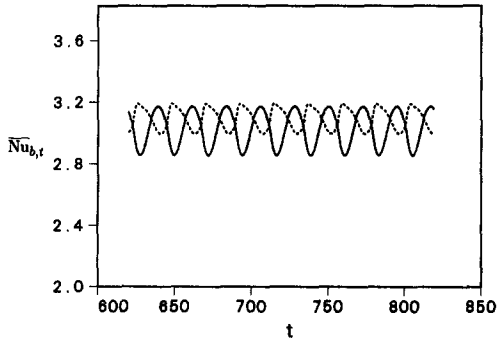

FIG. 10. Average Nusselt numbers from the lower hot surface (——) and the upper cold surface (– – –) of the channel, once the steady, periodic traveling waves have occurred. $Gr = 1.85 \times 10^5$, $Re = 30$, $L/H = 8$, and $\varepsilon = 2.333$.

ratio of the channel and are related to the thermal wave position at $x = L$. As the channel aspect ratio L/H is increased, the effects of the wave at $x = L$ on the average Nusselt numbers are less and the amplitudes of the variations in average Nusselt numbers become smaller. The temporal averages of the spatially averaged Nusselt numbers of Fig. 10 have attained constant values (the condition of stationarity as defined earlier has been realized).

Figure 11 shows the local Nusselt numbers at the hot and cold surfaces of the channel at $t = 700$. The fact that the average Nusselt number (cf. Fig. 10) is slightly larger at the cold surface than at the hot surface corresponds to the larger local Nusselt number at the cold surface near the inlet of the channel which is a result of the boundary conditions applied on the temperature and the velocity (adiabatic and parabolic, respectively) at $x = 0$. Note that for variable property flow a fully developed velocity profile is not symmetric about the midplane of the channel. When integrated over time, an overall energy balance for the channel shows that more energy is convected into the channel than is convected out of the channel; thus the overall energy balance is maintained. The local Nusselt numbers at $x = 0$ in Fig. 11 are significantly larger than 1.0 due to the effects of the variable properties.

Effect of the Grashof number. Starting with the stationary flow condition discussed above, values of Gr were increased to 3.5×10^5 and 5.0×10^5; all other parameters were held constant. The case of $Gr = 6.0 \times 10^5$ was started from $t = 0$. Figure 12 shows the average Nusselt numbers at the top and bottom surfaces of the channel and the temperature variation with time at the middle of the channel ($x = 4.0$, $y = 0.5$; $L/H = 8$) for these three values of Gr. These results are shown in Fig. 12 to be more complex and to have lower frequencies than the corresponding curves at the lower Grashof number of 1.85×10^5 that are shown in Figs. 9 and 10. The results of Figs. 12(a) and (b) were obtained on an (x, y) grid of (81, 21) points whereas those of Fig. 12(c) were obtained on an (x, y) grid of (121, 41) points. We note that the stationary condition defined above has been reached in all of the results shown in Fig. 12.

Consistent with the trend discussed earlier for the small temperature difference condition, the results for large temperature differences also show that as the Grashof number is decreased for fixed Re and L/H, the transverse, traveling waves appear further downstream from the entrance of the channel and, for a sufficiently small value of Gr, disappear altogether. Figure 13 shows the variation with time of the average Nusselt numbers on the channel surfaces when Gr is decreased from 1.85×10^5 to 7.5×10^4 at $t = 200$ for $Re = 30$, $L/H = 8$, and $\varepsilon = 2.333$. As the time increases, the transverse waves gradually diminish and the flow becomes steady. However, if the Grashof number is only decreased from 1.85×10^5 to 1.25×10^5 at $t = 200$, transverse, traveling waves now remain in the channel as seen in Fig. 14 which shows the local Nusselt numbers at $t = 300$. However, in comparing Figs. 14 and 11, we see that the initiation of the in-

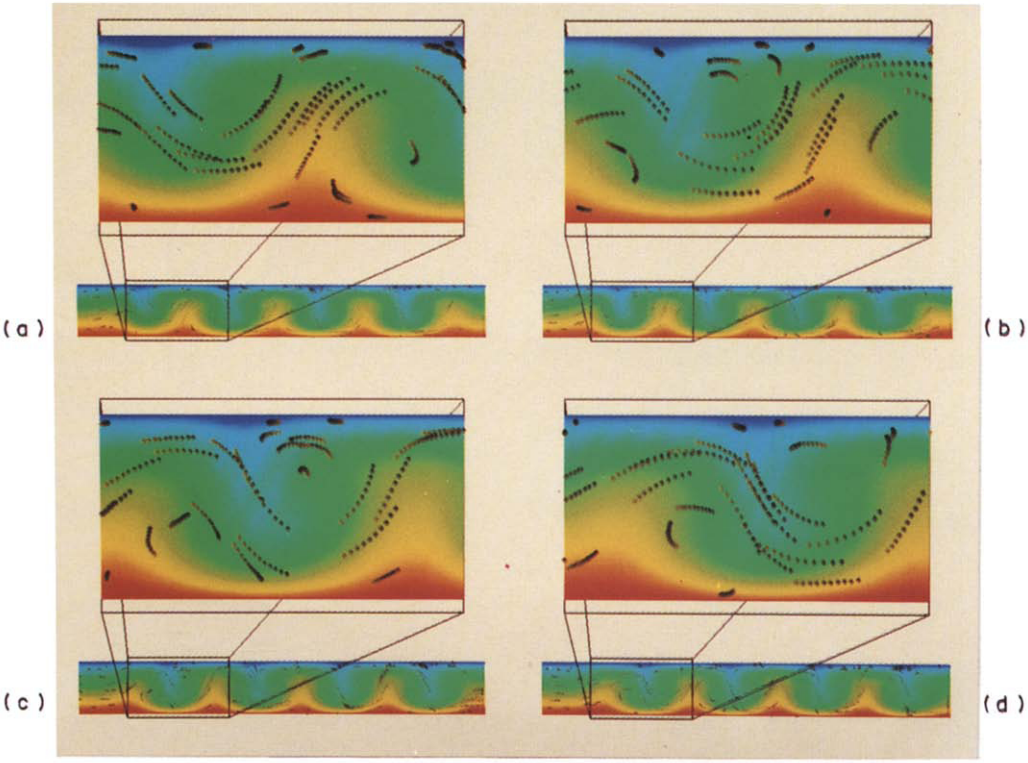

FIGS. 8(a)–(d). Color shading representing temperature and particles representing the velocity field in horizontal channel showing transverse waves traveling from left to right. Red, green, and blue correspond to high, intermediate, and low temperatures, respectively. Thermal wave movement: (a)–(d) correspond to $t = 340$, 343, 346, and 349, respectively. $Gr = 1.85 \times 10^5$, $Re = 30$, $L/H = 8$, and $\varepsilon = 2.333$; waves are periodic.

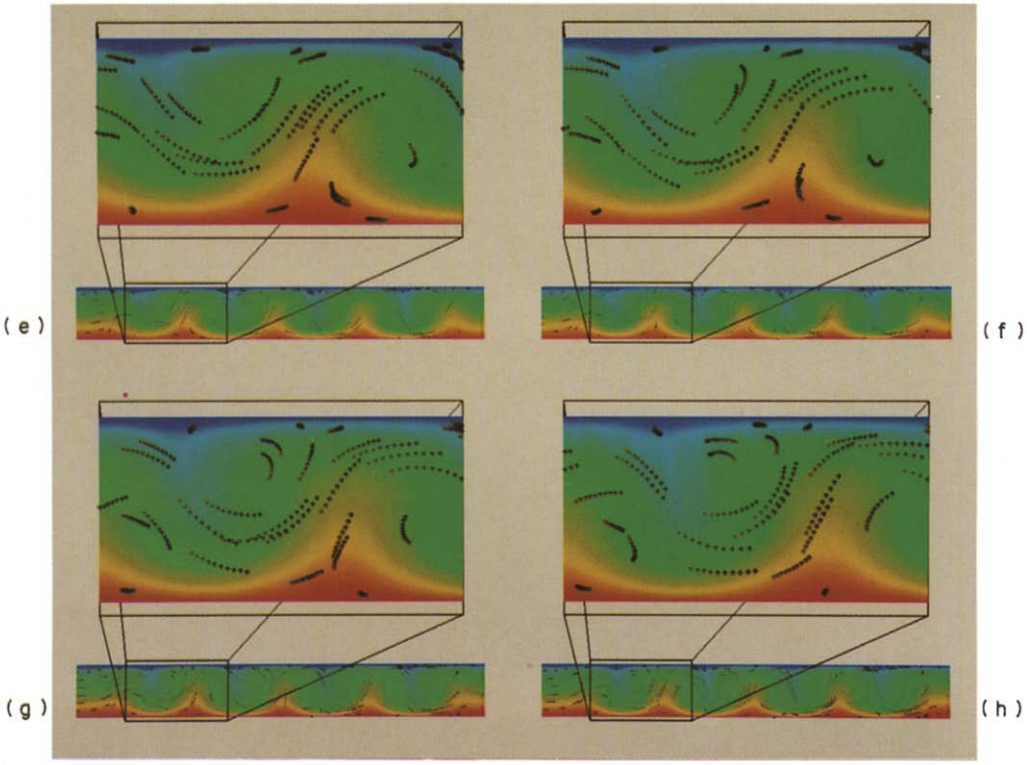

FIGS. 8(e)–(h). Color shading representing temperature and particles representing the velocity field in horizontal channel showing transverse waves traveling from left to right. Red, green, and blue correspond to high, intermediate, and low temperatures, respectively. Gas velocity: (e)–(h) correspond to $t = 340$, 341, 342, and 343, respectively. $Gr = 1.85 \times 10^5$, $Re = 30$, $L/H = 8$, and $\varepsilon = 2.333$; waves are periodic.

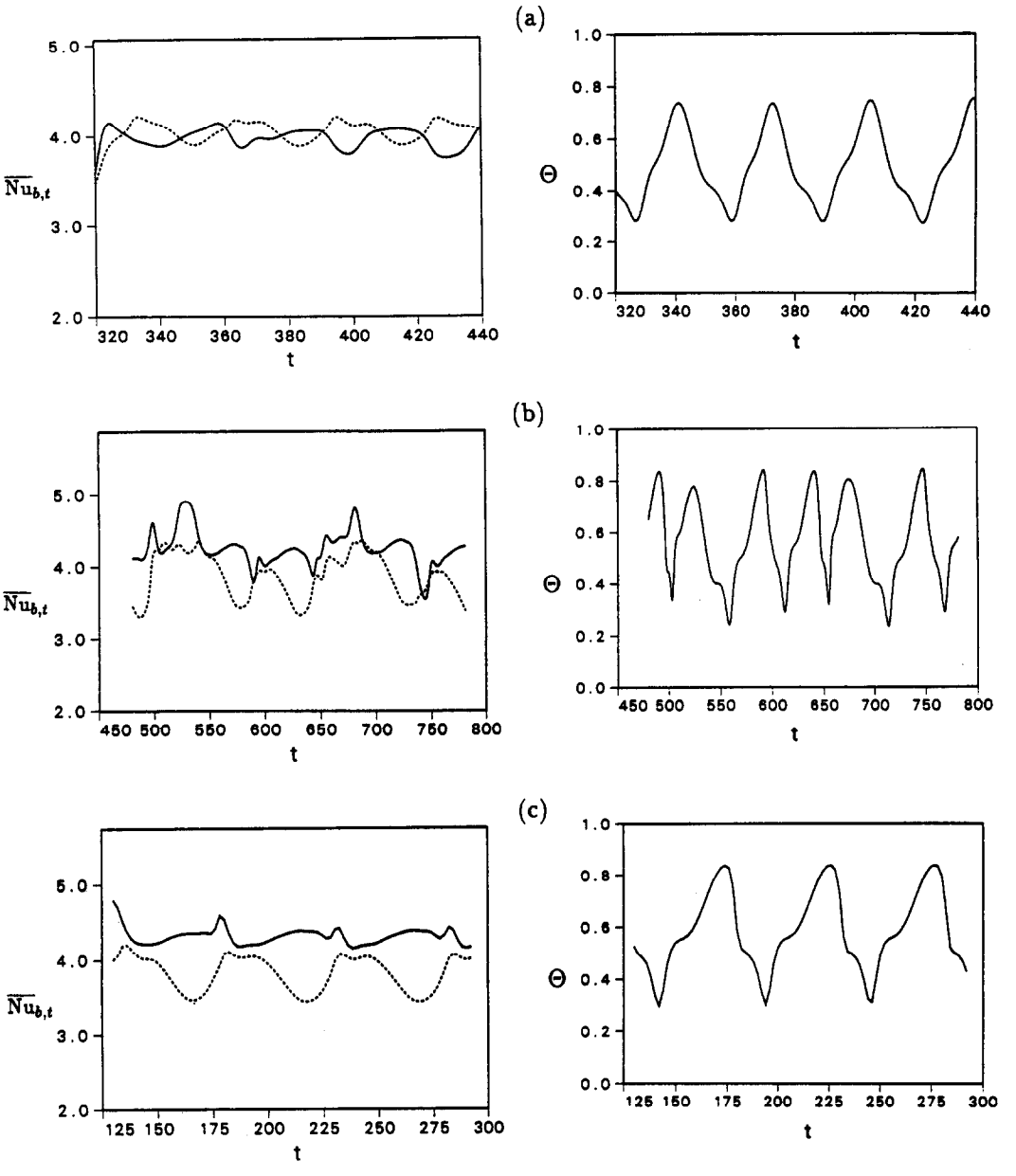

FIG. 12. Average Nusselt numbers at the channel surfaces, (——) hot surface, (– – –) cold surface; time history of temperature in the middle of the channel ($x = 4.0$, $y = 0.5$) for increasing Gr: (a) $Gr = 3.5 \times 10^5$; (b) $Gr = 5.0 \times 10^5$; (c) $Gr = 6.0 \times 10^5$. $Re = 30$, $L/H = 8$, and $\varepsilon = 2.333$.

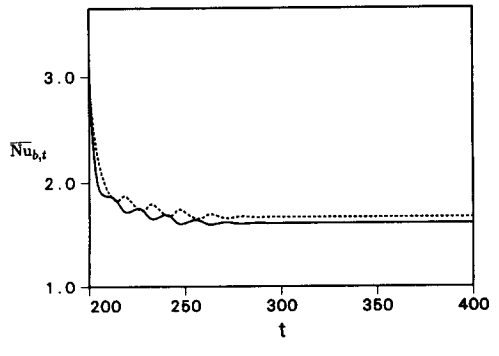

FIG. 13. Average heat fluxes from the lower hot surface (——) and the upper cold surface (– – –) of the channel upon decreasing Gr to 7.5×10^4 from 1.85×10^5 at $t = 200$; $Re = 30$, $L/H = 8$, and $\varepsilon = 2.333$.

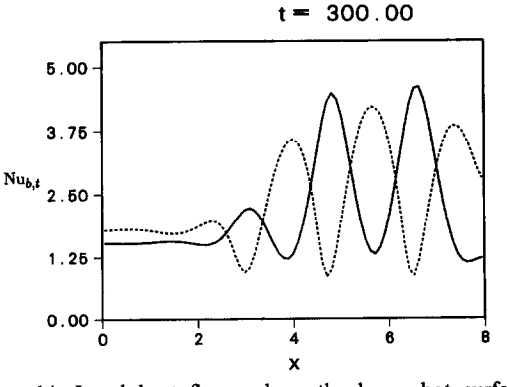

FIG. 14. Local heat fluxes along the lower hot surface (——) and the upper cold surface (– – –) of the channel after the average heat fluxes have become stationary. $Gr = 1.25 \times 10^5$, $Re = 30$, $L/H = 8$, and $\varepsilon = 2.333$.

stability occurs further downstream in Fig. 14 and there are fewer waves within the channel.

Effect of the Reynolds number. The effect of increasing Re on the position of the initiation of traveling, transverse waves is similar to that of decreasing Gr. By increasing the Reynolds number for fixed Gr, L/H, and ε, the instability appears further downstream, and if the channel is short enough the instability disappears, apparently being swept out of the channel. In Fig. 15, the local Nusselt numbers are shown for the case $Gr = 1.85 \times 10^5$, $Re = 50$, $L/H = 8$, $\varepsilon = 2.333$ at $t = 600$. The instability is confined to the downstream 30% of the channel. This is in contrast to Fig. 11 for which $Re = 30$. If the Reynolds number is increased further to $Re = 100$, the instability no longer exists in the channel as shown in the plot of the average Nusselt numbers in Fig. 16, where Re was changed from 30 to 100 at $t = 200$.

We note that Moffat and Jensen [8, 9] have studied

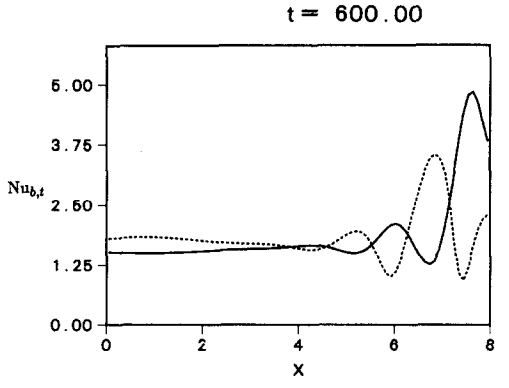

FIG. 15. Local heat fluxes along the lower hot surface (——) and the upper cold surface (– – –) of the channel after the average heat fluxes have become stationary. $Gr = 1.85 \times 10^5$, $Re = 50$, $L/H = 8$, and $\varepsilon = 2.333$.

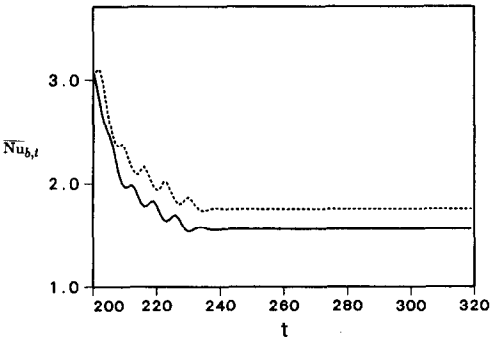

FIG. 16. Average heat fluxes from the lower hot surface (——) and the upper cold surface (– – –) of the channel upon increasing Re to 100 from 30 at $t = 200$. $Gr = 1.85 \times 10^5$, $L/H = 8$, and $\varepsilon = 2.333$.

the steady, parabolized, three-dimensional flow of hydrogen in a horizontal channel for $Gr = 1.87 \times 10^5$, $Re = 64$, $L/H = 5$, $\varepsilon = 3.41$, $W/H = 2$, with adiabatic conditions on the side walls. Steady, longitudinal rolls were predicted for these conditions. It is clear that a complete description of the flow phenomena over the entire range of Re that are of interest in CVD can be obtained only from an analysis of the transient, three-dimensional Navier–Stokes equations.

Effect of the aspect ratio. For small temperature differences, the aspect ratio L/H was shown to be an important parameter. Recall, that for small values of L/H, traveling waves may not be present even though the flow would be unstable at a larger value of L/H. A similar result holds for the variable property case. Specifically, for $Re = 50$, $Gr = 1.85 \times 10^5$, $L/H = 4$, and $\varepsilon = 2.333$ an instability did not develop (this is not shown). Extending the aspect ratio to $L/H = 8$ was shown in Fig. 15 to lead to an instability that was present for $x > 4$.

Comparison of average Nusselt numbers. In Table 1, we summarize the results for the time averages of

Table 1. Average Nusselt numbers, $(\overline{Nu}_{b,t})_{ta}$, in horizontal channel flow

ε	L/H	Re	Gr	$(\overline{Nu}_b)_{ta}$	$(\overline{Nu}_t)_{ta}$
0.0333	20	0.1	3000	1.1†	1.1†
0.0333	20	0.1	5000	1.65†	1.7†
0.0333	20	0.1	10 000	2.2†	2.3†
0.0333	40	40	15 000	1.72	1.72
0.0333	40	40	10 000	1.16	1.16
2.333	8	30	75 000	1.61‡	1.67‡
2.333	8	30	125 000	2.3	2.4
2.333	8	30	185 000	3.03	3.09
2.333	8	30	350 000	3.98	4.05
2.333	8	30	500 000	4.28	3.91
2.333	8	30	600 000	4.3	3.8
2.333	8	50	185 000	1.78	1.93
2.333	8	100	185 000	1.55‡	1.75‡
2.333	4	50	185 000	1.55‡	1.75‡

† Stationary state not achieved.

‡ Asymptotic values in the absence of waves. If fully developed, variable property velocity and temperature profiles had been specified at $x = 0$, these values would be the same on top and bottom surfaces and would be ≈ 1.63.

the spatially averaged Nusselt numbers, defined as

$$(\overline{Nu}_{b,t})_{ta} \equiv \frac{1}{(t_2 - t_1)} \int_{t_1}^{t_2} \overline{Nu}_{b,t}\, dt. \qquad (10)$$

The separate effects of increasing Re, decreasing Gr, or decreasing L/H are shown in Table 1 to result in smaller values of the Nusselt numbers. For the small temperature difference results ($\varepsilon = 0.0333$) with $Re = 0.1$, the average Nusselt numbers do not represent stationary values as defined earlier due to the extremely long time for the fluid to travel through the channel. For the cases of large temperature differences ($\varepsilon = 2.333$) without instability, the asymptotic values of the average Nusselt numbers on the top and bottom of the channel are not equal due to the small differences between the convective fluxes in and out of the channel. These small differences result from differences between the prescribed inlet boundary conditions for the velocity and temperature (equation (6), parabolic velocity profile and adiabatic temperature boundary condition) and the fully developed variable property profiles. At the highest values of Gr studied the average Nusselt numbers are more than 2.5 times larger than the conduction values in fully developed horizontal channel flow.

SUMMARY

We have predicted that transverse, traveling waves associated with the Rayleigh–Benard thermal instability occur for flow in a horizontal channel with a heated bottom surface and a cooled top surface. The local and the average Nusselt numbers from the heated and cooled surfaces of the channel have been determined. These solutions agree with the stability predictions of Gage and Reid, which are limited to the region of validity of the Boussinesq approximation and to infinite channels ($L/H \to \infty$). In addition, traveling, transverse waves are also predicted for the flow in a horizontal channel of finite length for conditions that are typical of CVD in which the Boussinesq approximation is not valid.

The results have been shown to depend on Re, Gr, L/H, and ε for helium. Increasing Gr leads to a more complex flow field with non-regular structure whereas decreasing Gr leads to the initiation of traveling waves further downstream. For small values of the Grashof number, traveling waves will not exist in the channel. Increasing Re also causes the transverse waves to occur further downstream, and for sufficiently large Re, there are no transverse waves in the channel. However, as noted in earlier studies, steady, longitudinal rolls do exist for certain values of Gr and Re in horizontal channels. For fixed Gr, Re, and ε, we have shown that increasing L/H can result in the occurrence of transverse, traveling waves whereas decreasing L/H can result in the elimination of these waves. We note that for cases where transverse, traveling waves occur, the heat transfer from the heated surface to the gas is increased from 50 to more than 300% over the amount transferred when the waves do not exist (i.e. the situation of fully developed velocity and temperature profiles in a horizontal channel flow).

For CVD applications the additional transfer resulting from the instability would significantly increase the deposition rate when operating a horizontal channel flow reactor in the transport limited regime. Furthermore, since the waves are traveling, any irregularities in the heat flux should be smoothed out over time. However, careful control over the reactor operating parameters would be required to avoid flow conditions which establish the steady, longitudinal vortices that have been noted in previous studies. Those flow instabilities would yield striations in the deposited material. Besides being of fundamental interest in respect to convective heat transfer this study should also help designers of CVD reactors gain a better understanding of the processes which occur in these systems.

Acknowledgements—The authors received much valuable help from S. Paolucci regarding the stability of low Reynolds number thermal convection. Continuing discussions with W. G. Breiland, M. E. Coltrin, A. W. Johnson and R. J. Kee on various aspects of CVD have been helpful and are appreciated. We thank R. A. Seban for his valuable comments. We are also indebted to V. K. Gabrielson for providing color movie graphics. This work was supported by the United States Department of Energy.

REFERENCES

1. K. F. Jensen, Modeling of chemical vapor deposition reactors, *Proc. 9th Int. Conf. on Chemical Vapor Deposition*, pp. 3–20 (1984).
2. L. J. Giling, Gas flow patterns in horizontal epitaxial reactor cells observed by interference holography, *J. Electrochem. Soc.* **129**(3), 634–644 (1982).
3. M. E. Coltrin, R. J. Kee and J. A. Miller, A mathematical model of the coupled fluid mechanics and chemical kinetics in a chemical vapor deposition reactor, *J. Electrochem. Soc.* **131**(2), 425–434 (1984).
4. S. Ostrach, Fluid mechanics in crystal growth—The 1982 Freeman Scholar Lecture, *J. Fluids Engng* **105**, 5–20 (1983).
5. R. Pollard and J. Newman, Silicon deposition on a rotating disk, *J. Electrochem. Soc.* **127**(3), 744–752 (1980).
6. M. E. Coltrin, R. J. Kee, G. H. Evans and J. A. Miller, Theoretical modeling of the fluid mechanics and gas-phase chemistry in a rotating-disk chemical vapor deposition reactor, *Proc. Tenth Int. Conf. on Chemical Vapor Deposition* (Edited by G. W. Cullen), pp. 33–41. The Electrochemical Society (1987).
7. G. W. Cullen (Editor), *Proc. Tenth Int. Conf. on Chemical Vapor Deposition*, pp. 11–32, 175–180, 193–203. The Electrochemical Society (1987).
8. H. Moffat and K. F. Jensen, Complex flow phenomena in MOCVD reactors, *J. Crystal Growth* **77**, 108–119 (1986).
9. H. Moffat and K. F. Jensen, Three-dimensional flow effects in silicon CVD in horizontal reactors, *J. Electrochem. Soc.* **135**(2), 459–471 (1988).
10. C. Houtman, D. B. Graves and K. F. Jensen, CVD in stagnation point flow, *J. Electrochem. Soc.* **133**(5), 961–970 (1986).

11. J. van de Ven, G. M. J. Rutten, M. J. Raaijmakers and L. J. Giling, Gas phase depletion and flow dynamics in horizontal MOCVD reactors, *J. Crystal Growth* **76,** 352–372 (1986).
12. K. C. Chiu and F. Rosenberger, Mixed convection between horizontal plates—1. Entrance effects, *Int. J. Heat Mass Transfer* **30,** 1645–1654 (1987).
13. B. J. Curtis and J. P. Dismukes, Effects of natural and forced convection in vapor phase growth systems, *J. Crystal Growth* **17,** 128–140 (1972).
14. K. C. Chiu, J. Ouazzani and F. Rosenberger, Mixed convection between horizontal plates—2. Fully developed flow, *Int. J. Heat Mass Transfer* **30,** 1655–1662 (1987).
15. Y. Mori and Y. Uchida, Forced convective heat transfer between horizontal flat plates, *Int. J. Heat Mass Transfer* **9,** 803–817 (1966).
16. M. Akiyama, G. J. Hwang and K. C. Cheng, Experiments on the onset of longitudinal vortices in laminar forced convection between horizontal plates, *Trans. ASME, J. Heat Transfer* 335–341 (Nov. 1971).
17. Y. Kamotani and S. Ostrach, Effect of thermal instability on thermally developing laminar channel flow, *Trans. ASME, J. Heat Transfer* 62–66 (Feb. 1976).
18. F. P. Incropera and J. A. Schutt, Numerical simulation of laminar mixed convection in the entrance region of horizontal rectangular ducts, *Numer. Heat Transfer* **8,** 707–729 (1985).
19. Y. Kamotani, S. Ostrach and H. Miao, Convective heat transfer augmentation in thermal entrance regions by means of thermal instability, *Trans. ASME, J. Heat Transfer* **101,** 222–226 (1979).
20. K. J. Kennedy and A. Zebib, Combined forced and free convection between parallel plates, *Heat Transfer 1982, Proc. 7th Int. Heat Transfer Conf.*, Munich, Vol. 3, pp. 447–451 (1982).
21. S. H. Davis, Convection in a box: linear theory, *J. Fluid Mech.* **30**(3), 465–478 (1967).
22. K. Stork and U. Müller, Convection in boxes: experiments, *J. Fluid Mech.* **54**(4), 599–611 (1972).
23. K. Chandra, Instability of fluids heated from below, *Proc. R. Soc. Lond. Ser. A* **164,** 231–242 (1938).
24. D. Brunt, Experimental cloud formation. In *Compendium of Meteorology*, pp. 1255–1262. American Meteorological Society, Boston (1951).
25. K. S. Gage and W. H. Reid, The stability of thermally stratified plane Poiseuille flow, *J. Fluid Mech.* **33**(1), 21–32 (1968).
26. J. K. Platten and J. C. Legros, *Convection in Liquids*, Chap. 8. Springer, Berlin (1984).
27. J.-M. Luijkx, J. K. Platten and J. C. Legros, On the existence of thermoconvective rolls, transverse to a superimposed mean Poiseuille flow, *Int. J. Heat Mass Transfer* **24,** 1287–1291 (1981).
28. S. Paolucci, On the filtering of sound from the Navier–Stokes equations, Sandia National Laboratories Report SAND82-8257 (1982).
29. A. D. Gosman and W. M. Pun, Calculation of recirculating flow, Lecture Notes, Imperial College of Science and Technology, London (1973).
30. S. V. Patankar, *Numerical Heat Transfer and Fluid Flow*. McGraw-Hill, New York (1980).
31. G. Evans and R. Greif, A numerical model of the flow and heat transfer in a rotating disk chemical vapor deposition reactor, *J. Heat Transfer* **109,** 928–935 (1987).

UNE ETUDE DES INSTABILITES D'ONDE PROGRESSIVE DANS UN ECOULEMENT EN CANAL HORIZONTAL AVEC APPLICATIONS AU DEPOT CHIMIQUE DE VAPEUR

Résumé—On étudie l'écoulement et le transfert thermique de l'hélium dans un canal horizontal de hauteur H et de longueur L, avec la surface inférieure chaude et la surface supérieure refroidie. Les solutions numériques des équations bidimensionnelles de Navier–Stokes et d'énergie en régime variable révèlent que pour des conditions intéressantes du dépôt chimique de vapeur (CVD), une instabilité thermique dans le fluide (instabilité de Rayleigh–Benard), produite par la différence de température entre les deux surfaces, peut conduire à des ondes progressives transversales. Les résultats montrent les effets de ces ondes progressives transversales. Les résultats montrent les effets de ces ondes sur l'écoulement et sur le transfert de chaleur, dans un domaine de nombre de Reynolds $Re = \bar{u}H/\nu_0$ ($10^{-1} < Re < 10^2$), de nombre de Grashof $Gr = g\varepsilon H^3/\nu_0^2$ ($2{,}5 \times 10^3 < Gr < 6{,}0 \times 10^5$), de rapport de forme L/H ($4 < L/H < 50$), pour deux rapports de température $\varepsilon = (T_s - T_0)/T_0$, 0,0333 et 2,333 qui correspondent respectivement à des écoulements à propriétés constantes et variables. L'existence des ondes progressives transversales augmente le transfert de chaleur à 50% à plus de 300% par rapport au cas sans ondes progressives. L'effet important du rapport de forme sur les résultats est dégagé.

UNTERSUCHUNG VON WANDERWELLEN-INSTABILITÄTEN IN EINER HORIZONTALEN KANALSTRÖMUNG BEI DER CHEMISCHEN DAMPFABSCHEIDUNG

Zusammenfassung—Strömung und Wärmetransport von Helium in einem horizontalen Kanal der Höhe H und der Länge L mit beheizter Boden- und gekühlter Deckfläche werden untersucht. Die numerische Lösung der instationären zweidimensionalen Navier–Stokes- und Energiegleichungen zeigt, daß unter den für die chemische Dampfabscheidung interessierenden Bedingungen die thermische Instabilität im Fluid (Rayleigh–Bénard-Instabilität) zu wandernden transversalen Wellen führen kann. Die Ergebnisse zeigen den Einfluß dieser Wellen auf die Strömung und den Wärmetransport für Reynolds-Zahlen $Re = \bar{u}H/\nu_0$ ($10^{-1} < Re < 10^2$), Grashof-Zahlen $Gr = g\varepsilon H^3/\nu_0^2$ ($2{,}5 \times 10^3 < Gr < 6{,}0 \times 10^5$), Seitenverhältnisse L/H ($4 < L/H < 50$) bei zwei Temperaturverhältnissen $\varepsilon = (T_s - T_0)/T_0$ (0,0333 und 2,333), die einer Strömung mit konstanten bzw. variablen Stoffwerten entsprechen. Es zeigt sich, daß das Auftreten der wandernden transversalen Wellen den Wärmetransport zwischen 50 und über 300% erhöht. Der wichtige Einfluß, den das Seitenverhältnis auf die Ergebnisse ausübt, wird ebenfalls dargestellt.

ИССЛЕДОВАНИЕ НЕУСТОЙЧИВОСТИ В ВИДЕ БЕГУЩИХ ВОЛН ПРИ ТЕЧЕНИИ В ГОРИЗОНТАЛЬНОМ КАНАЛЕ ПРИМЕНТЕЛЬНО К ХИМИЧЕСКОМУ ОСАЖДЕНИЮ ПАРА

Аннотация—Исследуются течение и теплоперенос гелия в горизонтальном канале высотой H и длиной L с нагреваемой нижней и охлаждаемой верхней поверхностями. Численные решения нестационарных двумерных уравнений Навье–Стокса и сохранения энергии показывают, что в рассматриваемых условиях химического осаждения пара тепловая неустойчивость текучей среды (неустойчивость Рэлея–Бенара), вызванная разностью температур горизонтальных поверхностей канала, может привести к появлению бегущих поперечных волн. Результаты показывают влияние этих волн на течение и теплоперенос для диапазона изменения чисел Рейнольдса $Re = \bar{u}H/\nu_0$ ($10^{-1} < Re < 10^2$), чисел Грасгофа $Gr = g\varepsilon H^3/\nu_0^2$ ($2{,}5 \times 10^3 < Gr < 6{,}0 \times 10^5$), отношения сторон L/H ($4 < L/H < 50$), для двух отношений температур $\varepsilon = (T_s - T_0)/T_0$, равных 0,0333 и 2,333 и соответствующим постоянным и переменным свойствам течения. Показано, что появление поперечных бегущих волн увеличивает теплоперенос от 50% до более чем 300% по сравнению со случаем, когда их нет. Подчеркивается также сильное влияние отношения L/H канала на результаты.